NANO LETTERS

Letter

pubs.acs.org/NanoLett

Band Structure Engineering in Topological Insulator Based Heterostructures

T. V. Menshchikova,*[,†] M. M. Otrokov,[‡,†] S. S. Tsirkin,[‡,†] D. A. Samorokov,[†] V. V. Bebneva,[†] A. Ernst,[§,∥] V. M. Kuznetsov,[†] and E. V. Chulkov[‡,⊥]

[†]Tomsk State University, pr. Lenina 36, 634050 Tomsk, Russia

[‡]Donostia International Physics Center (DIPC), P. Manuel de Lardizabal 4, 20018 San Sebastián, Basque Country, Spain

[§]Max-Planck-Institut für Mikrostrukturphysik, Weinberg 2, D-06120 Halle, Germany

[∥]Wilhelm Ostwald Institut für Physikalische und Theoretische Chemie, Universität Leipzig, Linnéstraße 2, D-04103 Leipzig, Germany

[⊥]Departamento de Física de Materiales, Facultad de Ciencias Químicas, UPV/EHU and Centro de Física de Materiales (CFM) (CSIC-UPV/EHU), Apdo. 1072, 20080 San Sebastián, Basque Country, Spain

Supporting Information

ABSTRACT: The ability to engineer an electronic band structure of topological insulators would allow the production of topological materials with tailor-made properties. Using ab initio calculations, we show a promising way to control the conducting surface state in topological insulator based heterostructures representing an insulator ultrathin films on the topological insulator substrates. Because of a specific relation between work functions and band gaps of the topological insulator substrate and the insulator ultrathin film overlayer, a sizable shift of the Dirac point occurs resulting in a significant increase in the number of the topological surface state charge carriers as compared to that of the substrate itself. Such an effect can also be realized by applying the external electric field that allows a gradual tuning of the topological surface state. A simultaneous use of both approaches makes it possible to obtain a topological insulator based heterostructure with a highly tunable topological surface state.

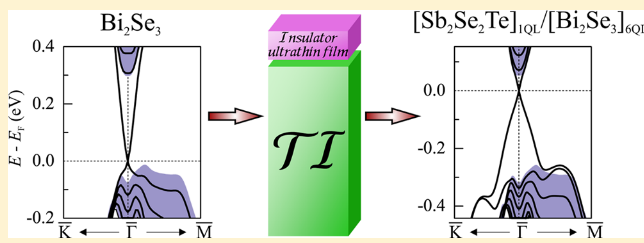

KEYWORDS: *Topological insulators, electronic structure, heterostructures, electric field*

Topological insulators (TIs) are novel materials, demonstrating a fundamental interplay between electronic structure and topology, as well as providing a platform for potentially promising applications in spintronics.[1,2] Up to date, the unique fingerprint of this class of materials, that is, spin-polarized gapless surface state with linear dispersion, has been experimentally confirmed for a number of compounds containing heavy elements like Bi, Te, Pb, and Sb.[3−15] These include random alloys,[3] binary,[4−7] and ternary[8−10] layered compounds, as well as the thallium-based compounds.[11−14]

Intended to design materials with tailor-made properties, the band structure engineering in TIs acquires a growing importance.[8,16−20] In particular, the variation of the atomic composition has recently been used to synthesize TIs with a truly insulating bulk and a tunable Dirac point (DP) across the band gap.[17−19] Another promising strategy that allows the modification of the TI spectrum is the deposition of an insulator ultrathin film (IUF) on top of the TI surface. It was shown that such an approach can be used to position the DP within the TI bulk band gap,[20] but a particular choice of the IUFs (single stoichiometric ZnS, ZnSe, and ZnTe layers) leads to the appearance of the trivial overlayer states at the Fermi level in the Bi_2Se_3 and Bi_2Te_3 band gaps.

In the present study, we propose a new way to design the IUF/TI heterostructures, consisting of a single tetradymite-type quintuple (QL) or septuple (SL) layer blocks on top of the TI substrates. Constructed in such a way, the heterostructures are guaranteed against appearance of the trivial Shockley-type surface states due to the chemical inertness of the IUF overlayer. Using ab initio simulations, we show that depending on the relation of work functions of TI and IUF a sizable upward or downward shift of the DP occurs, allowing for the rough control of the DP position. More importantly, the deposition of the IUF on top of the TI surface can lead to a substantial increase in the number of the topological surface state (TSS) charge carriers as compared to that of the TI substrate. Moreover, we show that essentially the same effect can be achieved by applying an external electric field, which enables a gradual tuning of the TSS. A simultaneous use of both approaches makes it possible to obtain a TI-based heterostructure with a highly tunable TSS.

The compounds used as constituents of the IUF/TI heterostructures are reported in Table 1. All of them possess

Received: September 4, 2013
Revised: November 14, 2013
Published: November 25, 2013

Table 1. The Structural and Energetic Characteristics of the IUF/TI Pairs Given in the X_1/X_2 Format (except for the Lattice Mismatch, Δ) with X_i Being Either Experimental Lattice Parameter, a_i, or Calculated Work Function, Φ_i, with the Indication of the Films Thicknesses, or Calculated Band Gap, E_i (i = 1,2)[a]

IUF/TI	a_1(Å)/a_2(Å)	Δ (%)	Φ_1(eV)/ Φ_2(eV)	E_1(eV)/ E_2(eV)
$[Sb_2Se_2Te]_{1QL}/[Bi_2Se_3]_{6QL}$	4.105/4.114	−0.22	5.46(1QL)/ 5.42(6QL)	0.66/0.30
$[Sb_2Te_3]_{1QL}/[PbBi_2Te_2S_2]_{5SL}$	4.250/4.230	+0.47	4.80(1QL)/ 4.98(5SL)	0.48/0.34
$[PbBi_2Te_2S_2]_{1SL}/[Sb_2Te_3]_{6QL}$	4.230/4.250	−0.47	5.24(1SL)/ 4.49(6QL)	0.35/0.09
$[SnSb_2Te_4]_{1SL}/[Bi_2Te_2S]_{6QL}$	4.294/4.316	−0.51	4.79(1SL)/ 5.15(6QL)	0.39/0.27
$[Bi_2Te_2S]_{1QL}/[SnSb_2Te_4]_{5SL}$	4.316/4.294	+0.51	5.36(1QL)/ 4.45(5SL)	0.30/0.11
$[BiSbTe_2S]_{1QL}/[Sb_2Te_2S]_{6QL}$	4.197/4.170	+0.63	4.99(1QL)/ 4.58(6QL)	0.39/0.29

[a]Note that band gap values, E_i, are given for slab and bulk in the IUF (i = 1) and TI (i = 2) case, respectively.

a tetradymite-type structures in which QL or SL blocks are separated by the van der Waals gaps.[21−27] Note that unlike the rest of the compounds listed in Table 1, Sb_2Se_2Te is topologically trivial (see Supporting Information S1). Because most of the IUFs under consideration are building blocks of three-dimensional TIs, it must be emphasized that a single QL (or SL) of a three-dimensional TI compound has a gapped spectrum with no two-dimensional metallic states. The IUF/TI heterostructures were simulated within a model of repeating slabs separated by a vacuum gap of a minimum of 10 Å. The IUF overlayers were symmetrically attached to both sides of the substrate slab to preserve the inversion. To simulate an external electric field, a sawtooth-like potential was applied along the Cartesian z-axis. As it can be seen in Table 1, the lattice mismatch for each IUF/TI pair does not exceed 0.63% ensuring that heterostructures can be easily produced by molecular-beam epitaxy. The in-plane lattice parameters of the IUF/TI systems were fixed to the experimental ones of corresponding TIs, while the interlayer distances were optimized for the whole slab. It is implied throughout the paper, that the first ingredient of the IUF/TI system represents an IUF overlayer, while the second one corresponds to a TI substrate. For instance, the $[Sb_2Se_2Te]_{1QL}/[Bi_2Se_3]_{6QL}$ heterostructure represents the 1QL-thick Sb_2Se_2Te overlayer on top of the 6QL-thick Bi_2Se_3 slab (Figure 1a). For the sake of brevity, the subscripts indicating the thicknesses of the TI substrate and the IUF overlayer will be omitted below.

Figure 1b shows the Bi_2Se_3 TSS with the DP located at the Fermi level. Placing an Sb_2Se_2Te QL over the Bi_2Se_3 surface induces a fundamental modification of the spectrum: the DP shifts toward the conduction band minimum, the lower part of the Dirac cone becomes much larger and, respectively, the upper part gets much smaller, see Figure 1c. To the best of our knowledge, there is no TI characterized by such a type of dispersion. For the Sb_2Se_2Te/Bi_2Se_3 heterostructure, the number of the TSS charge carriers was evaluated by calculation of the group velocity. The analysis shows that the presence of the Sb_2Se_2Te QL on top of the Bi_2Se_3 surface leads to the essential decrease in the group velocity (from ∼3 eV/$Å^{-1}$ to ∼1.3 eV/$Å^{-1}$) and therefore to the increase in the number of the TSS charge carriers as compared to that of Bi_2Se_3.

The inset in Figure 1c shows spin-resolved constant energy contours taken at −90, −160, and −250 meV below the DP in Sb_2Se_2Te/Bi_2Se_3, that is, for the lower part of the cone. One can see that the contours have a circular shape down to −90 meV (as in the case of Bi_2Se_3 within 90 meV above the DP, Figure 1b), while below this level the hexagonal warping appears, which can lead to intraband backscattering.[5,7,28] However, it is evident that the perimeter of the Dirac cone section within −90 meV below the DP of Sb_2Se_2Te/Bi_2Se_3 is roughly two times higher than that of Bi_2Se_3 in a similar energy range above the DP. We stress that this quantity determines the number of the TSS charge carriers which in turn is directly related to the conductivity.

An interesting feature of the Sb_2Se_2Te/Bi_2Se_3 heterostructure is a significant increase in the thickness of the conducting layer as compared to that of Bi_2Se_3 (Figure 1d). It can be seen in Figure 1e that approximately 50% of the DP charge density is localized in the Sb_2Se_2Te overlayer, reaching its maximum near the Sb_2Se_2Te/Bi_2Se_3 interface. Also worth noticing is the

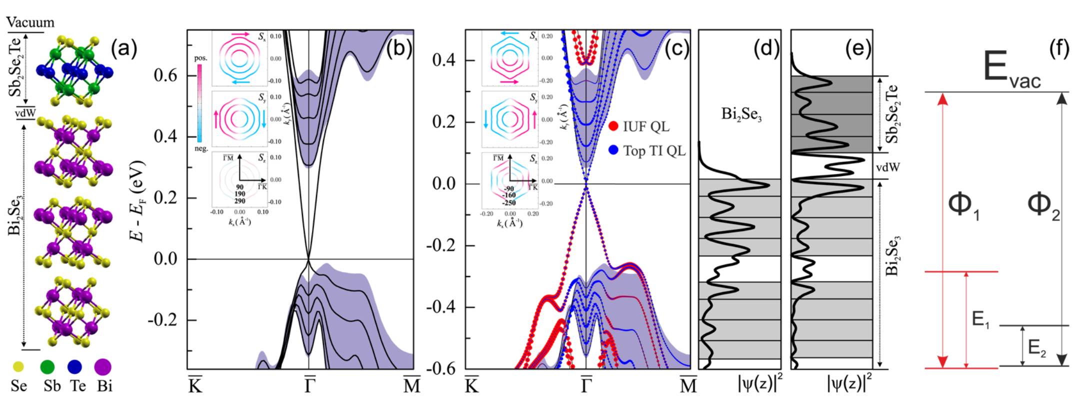

Figure 1. Crystal and electronic structure of Sb_2Se_2Te/Bi_2Se_3. (a) Atomic structure of Sb_2Se_2Te/Bi_2Se_3. (b,c) Surface band spectra of Bi_2Se_3 (b) and Sb_2Se_2Te/Bi_2Se_3 (c) with insets showing the Dirac cones spin textures represented by projections of spin vector $\vec{S}$ on Cartesian axes at different energies given with respect to the DPs. Blue-shaded areas correspond to the bulk band structure projected onto the surface Brillouin zone. The size of red and blue circles in panel (c) reflects the weight of the state in the Sb_2Se_2Te QL and in the top Bi_2Se_3 QL, respectively. (d,e) Spatial distribution of the DP charge density integrated over (x, y) plane for Bi_2Se_3 (d) and Sb_2Se_2Te/Bi_2Se_3 (e). (f) Schematic view of the band alignment of the Bi_2Se_3 substrate and the Sb_2Se_2Te QL. E_{vac} is the vacuum energy level, Φ_1 (Φ_2) and E_1 (E_2) are work functions and band gaps of the overlayer (substrate), respectively. See also the caption to Table 1 for more details.

dx.doi.org/10.1021/nl403312y | Nano Lett. 2013, 13, 6064−6069

emergence of the quantum well state in the conduction band local gap at ∼400 meV that is the Bychkov-Rashba split[29] and is mostly localized in the Sb_2Se_2Te overlayer. Note that the attachment of the additional Sb_2Se_2Te QL on top of $[Sb_2Se_2Te]_{1QL}/[Bi_2Se_3]_{6QL}$ leads to a degradation of the surface spectrum; the DP shifts even more toward the conduction band minimum, the dispersion of the lower part of the cone becomes more anisotropic, and a trivial state appears inside the fundamental band gap (see Supporting Information S2).

The modification of the TSS upon deposition of the IUF on top of the TI is directly connected to the relation of work functions and band gaps of the corresponding TI and IUF (Table 1). It is clearly seen in Figure 1f that the valence band maxima of Bi_2Se_3 and Sb_2Se_2Te QL are close to each other and that the TI band gap is built into the IUF one. The strong hybridization between the Bi_2Se_3 TSS and the Sb_2Se_2Te valence band states results in the upward shift of the DP. A similar effect was found in the $Sb_2Te_3/PbBi_2Te_2S_2$ (see Supporting Information S3) and $SnSb_2Te_4/Bi_2Te_2S$ heterostructures (Figure 2) despite the fact that the DP in Bi_2Te_2S lies below the valence band maximum. In the case of $SnSb_2Te_4/Bi_2Te_2S$, one difference takes place: band gaps of TI and IUF do not overlap but the IUF conduction band minimum is still located significantly higher than that of TI.

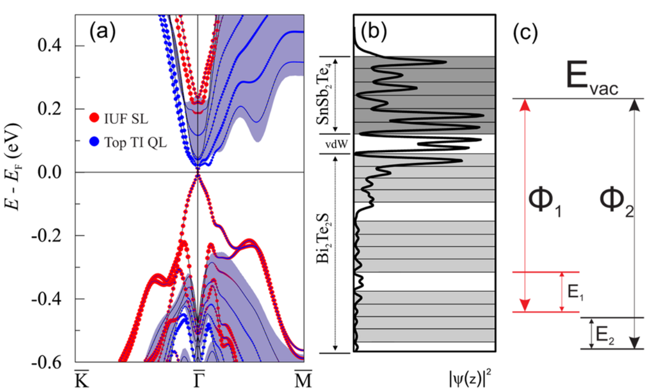

Figure 2. Peculiarities of the $SnSb_2Te_4/Bi_2Te_2S$ electronic structure. (a) Surface band structure. The color coding corresponds to the one used in Figure 1c. (b) Spatial distribution of the DP charge density integrated over (x, y) plane. (c) Schematic view of the band alignment of the Bi_2Te_2S substrate and the $SnSb_2Te_4$ SL.

Thus, our design of the Sb_2Se_2Te/Bi_2Se_3, $SnSb_2Te_4/Bi_2Te_2S$, and $Sb_2Te_3/PbBi_2Te_2S_2$ heterostructures preserves the advantages of the corresponding TI substrates leading neither to appearance of the trivial bands at the Fermi level nor to the decrease of the fundamental band gap, as it takes place in refs 20 and 30, respectively. More importantly, a substantial increase in the numbers of the TSSs charge carriers (as compared to those of the TI substrates) is expected in these systems.

Let us now present examples of the TSS modifications characterized by even more dramatic increase in the number of charge carriers. Figure 3a shows electronic spectrum of the $PbBi_2Te_2S_2/Sb_2Te_3$ heterostructure superimposed with the Sb_2Te_3 bulk band structure projected onto the surface Brillouin zone. By comparing the $PbBi_2Te_2S_2/Sb_2Te_3$ spectrum to that of pure Sb_2Te_3 (see ref 31), one can recognize a relocation of the DP from the fundamental band gap to the local band gap of the bulk valence band. Noteworthy, for that part where the TSS dispersion is perfectly linear a maximal diameter of the TSS constant energy contour in $PbBi_2Te_2S_2/Sb_2Te_3$ is almost 5 times higher than that in pure Sb_2Te_3 and 1.5 times higher than that in Sb_2Se_2Te/Bi_2Se_3 (Figure 1c). The charge density distributions for the selected k-points are shown in Figure 3c. As it can be seen in panels for k_1 and k_2 points, the part of the TSS lying in the fundamental band gap is localized in the IUF overlayer having its maximum near the heterostructure surface. Although mainly locating in the IUF SL, the $\bar{\Gamma}$-point TSS charge density demonstrates a resonance-like behavior due to the DP proximity to the bulk continuum.

The situation very similar to that in $PbBi_2Te_2S_2/Sb_2Te_3$ is observed in $Bi_2Te_2S/SnSb_2Te_4$ (Figure 3d−f). Here, the number of the TSS charge carriers is even higher than in the case of $PbBi_2Te_2S_2/Sb_2Te_3$, which correlates with deeper location of the DP in the local valence band gap. By comparing Figure 3b,e, as well as taking a look at Table 1, one may notice a similar relation between work functions and band gaps of TI and IUF for these two heterostructures. Namely, in both cases band gaps of TI and IUF do not overlap and the IUF gap lies significantly lower in energy than that of TI. Concerning $Bi_2Te_2S/SnSb_2Te_4$, we would also like to draw attention to the trivial state locating in the $SnSb_2Te_4$ fundamental band gap and

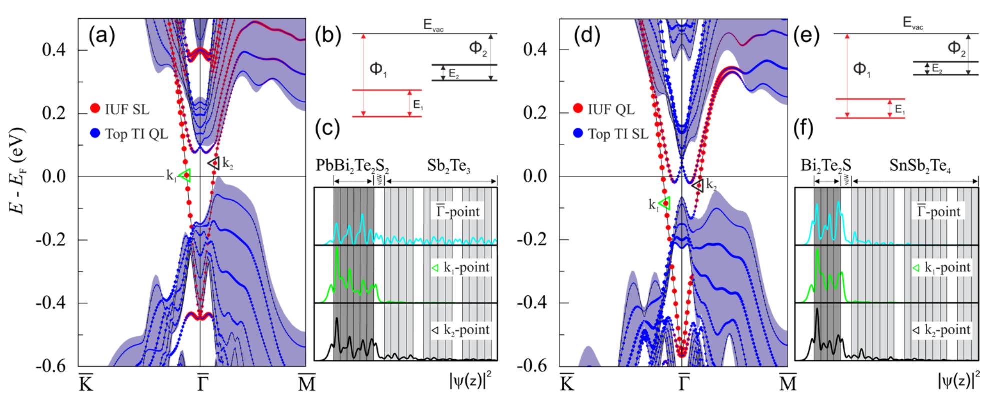

Figure 3. Peculiarities of the electronic structures of $PbBi_2Te_2S_2/Sb_2Te_3$ and $Bi_2Te_2S/SnSb_2Te_4$. (a,d) Surface band structures of $PbBi_2Te_2S_2/Sb_2Te_3$ and $Bi_2Te_2S/SnSb_2Te_4$, respectively. The color coding corresponds to that in Figure 1c. (b,e) Schematic view of the band alignment of the Sb_2Te_3 substrate and the $PbBi_2S_2Te_2$ SL (b) as well as of the $SnSb_2Te_4$ substrate and the Bi_2Te_2S QL (e). (c,f) Spatial distributions of the TSS charge density for $\bar{\Gamma}$, k_1, and k_2 points as integrated over (x, y) planes of $PbBi_2Te_2S_2/Sb_2Te_3$ and $Bi_2Te_2S/SnSb_2Te_4$, respectively. The k_1 and k_2 points are respectively marked by green and black triangles in panels (a) and (d).

dx.doi.org/10.1021/nl403312y | Nano Lett. 2013, 13, 6064−6069

crossing the Fermi level. Despite having quite characteristic shape, this state is not of the Bychkov−Rahsba-type because it remains almost unchanged upon switching-off the spin−orbit coupling. This state is essentially the second band of the free Bi_2Te_2S QL conduction band and appears in the heterostructure spectrum as a consequence of the specific band alignment of the $SnSb_2Te_4$ substrate and the Bi_2Te_2S QL. The presence of trivial states at the Fermi level of the TI-based heterostructure can have negative consequences for the topological transport. Below we offer an efficient way of the Fermi level clearance from such states.

Apart from two considered cases of the IUF/TI band alignment, there is another important scenario: the IUF conduction band minimum is situated near the TI valence band maximum. If this takes place, there is not any significant modification of the TSS dispersion in such a heterostructure as compared to that of the TI substrate. This case is exemplified by the $BiSbTe_2S/Sb_2Te_2S$ system whose band spectrum is shown in Figure 4a (see Supporting Information S4 for details

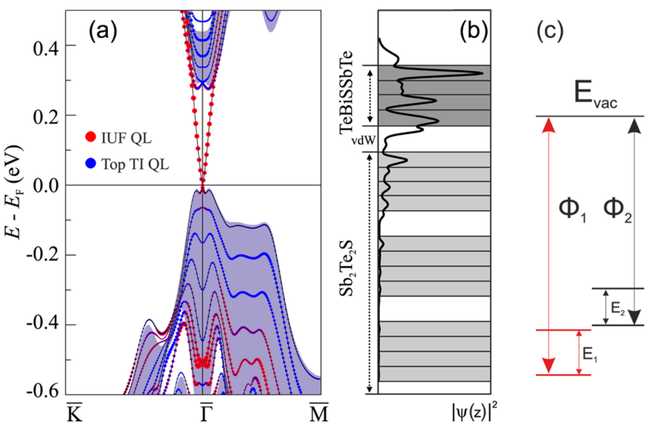

Figure 4. Peculiarities of the $BiSbTe_2S/Sb_2Te_2S$ electronic structure. (a) Surface band spectrum. The color coding corresponds to that in Figure 1c. (b) Spatial distribution of the DP charge density integrated over (x, y) plane. (c) Schematic view of the band alignment of the Sb_2Te_2S substrate and the $BiSbTe_2S$ QL.

about the $BiSbTe_2S/Sb_2Te_2S$ structure and the electronic spectra of the Sb_2Te_2S substrate and the $BiSbTe_2S$ QL). One can find that the Sb_2Te_2S TSS remains almost unchanged under deposition of the $BiSbTe_2S$ QL being shifted toward the bulk valence band by ~20 meV. Note that this value correlates well with the energy separation between the $BiSbTe_2S$ QL conduction band minimum and the Sb_2Te_2S slab valence band maximum (Table 1 and Figure 4c). Along with this, the DP charge density overflows into the $BiSbTe_2S$ QL and reaches its maximum near the heterostructure surface (Figure 4b). It is now worthwhile to compare the band alignment diagrams and the DP charge density distributions of all the heterosturctures under consideration. By doing so, the observation can be made that when the TSS hybridizes with the IUF overlayer conduction band, the DP charge density gets localized in the IUF overlayer. In contrast, the TSS hybridization with the overlayer valence band results in concentration of the DP charge density near the IUF/TI interface.

Let us now demonstrate that a gradual tuning of the DP position within the fundamental or local band gap can also be realized by means of the transverse electric field in the dual-gate geometry.[32,33] Within the model employed, applying an external electric field breaks the inversion symmetry thereby lifting the degeneracy of the TSS, which is manifested in the energy separation of the DPs belonging to different sides of the slab, as illustrated for Sb_2Se_2Te/Bi_2Se_3 in Figure 5a. Since the

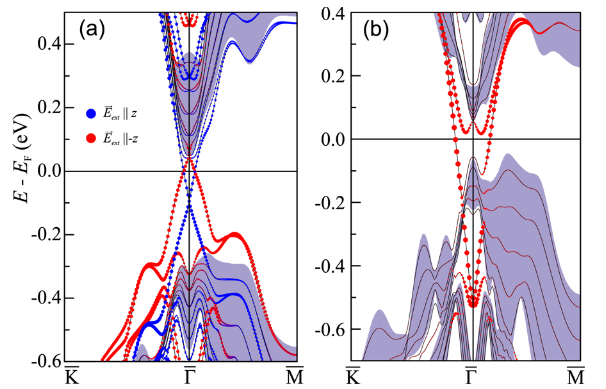

Figure 5. The effect of electric field on the electronic spectra of TI-based heterostructures. (a,b) Electronic spectra of Sb_2Se_2Te/Bi_2Se_3 (a) and $Bi_2Te_2S/SnSb_2Te_4$ (b) subjected to the external electric fields $\vec{E}_{ext}$ = (0,0, ± 0.03) V/nm and $\vec{E}_{ext}$ = (0,0,−0.01) V/nm, respectively. The size of blue (red) circles corresponds to the weight of the state in the top (bottom) IUF QL of the IUF/TI slab. In the alternative treatment, the bands highlighted by blue and red circles respectively correspond to the $\vec{E}_{ext} \| z$ and $\vec{E}_{ext} \| -z$ cases (see text).

bulklike states remain almost unaffected by the applied field, this separation means the change of the DP position inside the fundamental band gap. In case when the DP of the IUF/TI heterostructure resides in the local band gap of the bulk valence band, the application of the electric field results in a similar separation of the DPs. Noteworthy, we find that the energy separation of the DPs increases linearly with the strength of electric field (not shown). Therefore, the latter appears as a very efficient tool for the gradual tuning of the DP inside the bulk band gap. It is worth emphasizing that the TSS shift induced by the external electric field is rigid and therefore the linear dispersion of the TSS is preserved.

In the limit of thick TI films (six and more QLs) when the TSSs belonging to the different sides of the slab are decoupled, one can think about the manipulation not with two, but one DP. Indeed, the two TSSs shown in blue and red in Figure 5a can be considered as being located at the very same surface but corresponding to the different directions of the electric field, that is, to $\vec{E}_{ext} \| z$ and $\vec{E}_{ext} \| -z$, respectively. Thus, depending on the electric field direction, one can induce either upward or downward shift of the DP. This situation is rather similar to that of the DP shift induced by the deposition of the IUF overlayer on top of the TI surface. However, unlike the latter case, the use of the electric field allows a gradual tuning of the DP whose shift can be controlled in real time by changing the gate voltage. Moreover, by applying an external electric field of a corresponding strength and direction one can efficiently remove undesirable trivial surface states from the Fermi level. Indeed, as it can be seen in Figure 5b, where the spectrum of the gated $Bi_2Te_2S/SnSb_2Te_4$ is shown, the application of the electric field antiparallel to the surface normal ($\vec{E}_{ext} \| -z$) shifts trivial states toward the TI conduction band, cf. Figure 3d.

Thus, we have studied the electronic spectra of various heterostructures made of a single tetradymite-type quintuple or septuple layer blocks and topological insulator substrates. We have shown that depending on the relation of band gaps and

dx.doi.org/10.1021/nl403312y | Nano Lett. 2013, 13, 6064−6069

work functions of the topological insulator substrate and the insulator ultrathin film overlayer two scenarios are expected. The first one is characterized by a substantial modification of the topological surface state leading to a significant increase in the number of the surface state charge carriers as compared to that of the substrate. Such a modification stems from sizable shift of the Dirac point arising upon bringing the topological insulator in contact with the insulator ultrathin film and is accompanied by a partial or almost complete relocation of the topological surface state from the substrate to the overlayer. We stress that such a scenario is equally possible for the topological insulators with the Dirac point lying both above and below the bulk valence band maximum. In the second case, the topological surface state appears to be almost unchanged in the energy-momentum space, while in the real space it likewise relocates from the substrate to the overlayer. Furthermore, we have shown that applying transverse electric field it is possible to gradually change the Dirac point position across the topological insulator band gap, which can be done in real time. Finally, we have demonstrated that electric field can even be efficiently used to largely move trivial states from the Fermi level, which appear in some heterostructures due to specific overlayer/substrate band alignment. Combining the advantages of the two approaches described, one can obtain a topological insulator based heterostructure with a highly tunable topological surface state.

Methods. Electronic structure calculations were carried out within the density functional theory using the projector augmented-wave method[34] as implemented in the VASP code.[35,36] The exchange-correlation energy was treated using the generalized gradient approximation.[37] The Hamiltonian contained the scalar relativistic corrections and the spin−orbit coupling was taken into account by the second variation method.[38] In order to correctly describe the van der Waals interactions we made use of the DFT-D2 approach.[39]

ASSOCIATED CONTENT

Supporting Information

Atomic structure, bulk and surface electronic spectra of the trivial insulator Sb_2Se_2Te; peculiarities of the electronic structure of $[Sb_2Se_2Te]_{2QL}/[Bi_2Se_3]_{6QL}$, $[Sb_2Te_3]_{1QL}/[PbBi_2Te_2S_2]_{5SL}$, and $[BiSbTe_2S]_{1QL}/[Sb_2Te_2S]_{6QL}$. This material is available free of charge via the Internet at http://pubs.acs.org.

AUTHOR INFORMATION

Corresponding Author

*E-mail: menshikova_t@mail.ru.

Author Contributions

The calculations were performed mainly by T.V.M. with contributions by M.M.O., S.S.T., D.A.S., and V.V.B. The idea of the study was proposed by E.V.C., who is the supervisor of the project, and A.E. All authors contributed to discussion, data analysis, and manuscript editing. T.V.M., M.M.O., V.M.K., and E.V.C. wrote the manuscript.

Notes

The authors declare no competing financial interest.

ACKNOWLEDGMENTS

We acknowledge support by the Ministry of Education and Science of the Russian Federation (state task No. 2.8575.2013), the Federal Targeted Program "Scientific and scientific-pedagogical personnel of innovative Russia in 2009-2013" (No. 14.B37.21.1164) and Russian Foundation for Basic Research (Grant 13-02-12110 ofi_m). A.E. acknowledges funding by the German Research Foundation (DFG Grants ER 340/4-1 and the Priority Program 1666 "Topological Insulators"). Calculations were performed on the SKIF-Cyberia supercomputer of Tomsk State University. The authors also would like to thank Dr. S. V. Eremeev for useful discussion.

REFERENCES

(1) Hasan, M. Z.; Kane, C. L. Colloquium: Topological insulators. *Rev. Mod. Phys.* **2010**, *82*, 3045−3067.
(2) Qi, X.-L.; Zhang, S.-C. Topological insulators and superconductors. *Rev. Mod. Phys.* **2011**, *83*, 1057−1110.
(3) Hsieh, D.; et al. A topological Dirac insulator in a quantum spin Hall phase. *Nature* **2008**, *452*, 970−974.
(4) Xia, Y.; et al. Observation of a large-gap topological-insulator class with a single Dirac cone on the surface. *Nature Phys.* **2009**, *5*, 398−402.
(5) Chen, Y. L.; et al. Experimental realization of a three-dimensional topological insulator, Bi_2Te_3. *Science* **2009**, *325*, 178−181.
(6) Hsieh, D.; et al. Observation of time-reversal-protected single-Dirac-cone topological-insulator states in Bi_2Te_3 and Sb_2Te_3. *Phys. Rev. Lett.* **2009**, *103*, 146401.
(7) Kuroda, K.; et al. Hexagonally deformed Fermi surface of the 3D topological insulator Bi_2Se_3. *Phys. Rev. Lett.* **2010**, *105*, 076802.
(8) Eremeev, S. V.; et al. Atom-specific spin mapping and buried topological states in a homologous series of topological insulators. *Nat. Commun.* **2012**, *3*, 635.
(9) Kuroda, K.; et al. Experimental verification of $PbBi_2Te_4$ as a 3D topological insulator. *Phys. Rev. Lett.* **2012**, *108*, 206803.
(10) Okamoto, K.; et al. Observation of a highly spin-polarized topological surface state in $GeBi_2Te_4$. *Phys. Rev. B* **2012**, *86*, 195304.
(11) Sato, T.; et al. Direct evidence for the Dirac-cone topological surface states in the ternary chalcogenide $TlBiSe_2$. *Phys. Rev. Lett.* **2010**, *105*, 136802.
(12) Kuroda, K.; et al. Experimental realization of a three-dimensional topological insulator phase in ternary chalcogenide $TlBiSe_2$. *Phys. Rev. Lett.* **2010**, *105*, 146801.
(13) Chen, Y. L.; et al. Single Dirac cone topological surface state and unusual thermoelectric property of compounds from a new topological insulator family. *Phys. Rev. Lett.* **2010**, *105*, 266401.
(14) Souma, S.; et al. Spin polarization of gapped Dirac surface states near the topological phase transition in $TlBi(S_{1-x}Se_x)_2$. *Phys. Rev. Lett.* **2012**, *109*, 186804.
(15) Gehring, P.; et al. A Natural Topological Insulator. *Nano Lett.* **2013**, *13*, 1179−1184.
(16) Menshchikova, T. V.; Eremeev, S. V.; Koroteev, Yu M.; Kuznetsov, V. M.; Chulkov, E. V. Ternary compounds based on binary topological insulators as an efficient way for modifying the Dirac cone. *JETP Lett.* **2011**, *93*, 15−20.
(17) Zhang, J.; et al. Band structure engineering in $(Bi_{1-x}Sb_x)_2Te_3$ ternary topological insulators. *Nat. Commun.* **2011**, DOI: 10.1038/ncomms1588.
(18) Ren, Z.; Taskin, A. A.; Sasaki, S.; Segawa, K.; Ando, Y. Optimizing $Bi_{2-x}Sb_xTe_{3-y}Se_y$ solid solutions to approach the intrinsic topological insulator regime. *Phys. Rev. B* **2011**, *84*, 165311.
(19) Arakane, T.; et al. Tunable Dirac cone in the topological insulator $Bi_{2-x}Sb_xTe_{3-y}Se_y$. *Nat. Commun.* **2012**, DOI: 10.1038/ncomms1639.
(20) Wu, G.; et al. Tuning the vertical location of helical surface states in topological insulator heterostructures via dual-proximity effects. *Sci. Rep.* **2013**, *3*, 1233.
(21) Hulliger, F. *Structural chemistry of layer-type phases*; D. Reidel Pub. Co.: Dordrecht, 1976.
(22) Mishra, S. K.; Satpathy, S.; Jepsen, O. Electronic structure and thermoelectric properties of bismuth telluride and bismuth selenide. *J. Phys.: Condens. Matter* **1997**, *9*, 461−470.

(23) Grauer, D. C.; Hor, Y. S.; Williams, A. J.; Cava, R. J. Thermoelectric properties of the tetradymite-type Bi_2Te_2S-Sb_2Te_2S solid solution. *Mater. Res. Bull.* **2009**, *44*, 1926−1929.
(24) Liu, H.; Chang, L. L. Y. Lead and bismuth chalcogenide systems. *Am. Mineral.* **1994**, *79*, 1159.
(25) Silkin, I. V.; et al. Natural sulfur-containing minerals as topological insulators with a wide band gap. *JETP Lett.* **2012**, *96*, 322−325.
(26) Zhukova, T. B.; Zaslavskii, A. I. Crystal structures of the compounds $PbBi_4Te_7$, $PbBi_2Te_4$, $SnBi_4Te_7$, $SnBi_2Te_4$, $SnSb_2Te_4$, and $GeBi_4Te_7$. *Sov. Phys. Crystallogr.* **1972**, *16*, 796−800.
(27) Menshchikova, T. V.; Eremeev, S. V.; Chulkov, E. V. Electronic structure of $SnSb_2Te_4$ and $PbSb_2Te_4$ topological insulators. *Appl. Surf. Sci.* **2013**, *267*, 1−3.
(28) Fu, L. Hexagonal warping effects in the surface states of the topological insulator Bi_2Te_3. *Phys. Rev. Lett.* **2009**, *103*, 266801.
(29) Bychkov, Yu. A.; Rashba, E. I. Properties of a 2D electron gas with lifted spectral degeneracy. *JETP Lett.* **1984**, *39*, 78−81.
(30) Zhang, Q.; Zhang, Z.; Zhu, Z.; Schwingenschlögl, U.; Cui, Y. Exotic Topological Insulator States and Topological Phase Transitions in Sb_2Se_3-Bi_2Se_3 Heterostructures. *ACS Nano* **2012**, *6*, 2345−2352.
(31) Menshchikova, T. V.; Eremeev, S. V.; Chulkov, E. V. On the origin of two-dimensional electron gas states at the surface of topological insulators. *JETP Lett.* **2011**, *94*, 106−111.
(32) Yazyev, O. V.; Moore, J. E.; Louie, S. G. Spin polarization and transport of surface states in the topological insulators Bi_2Se_3 and Bi_2Te_3 from first principles. *Phys. Rev. Lett.* **2010**, *105*, 266806.
(33) Kim, M.; Kim, C. H.; Kim, H.-S.; Ihm, J. Topological quantum phase transitions driven by external electric fields in Sb_2Te_3 thin films. *Proc. Natl. Acad. Sci. U.S.A.* **2012**, *109*, 671−674.
(34) Blöchl, P. E. Projector augmented-wave method. *Phys. Rev. B* **1994**, *50*, 17953.
(35) Kresse, G.; Furthmüller, J. Efficient iterative schemes for ab initio total-energy calculations using a plane-wave basis set. *Phys. Rev. B* **1996**, *54*, 11169.
(36) Kresse, G.; Joubert, D. From ultrasoft pseudopotentials to the projector augmented-wave method. *Phys. Rev. B* **1999**, *59*, 1758.
(37) Perdew, J. P.; Burke, K.; Ernzerhof, M. Generalized gradient approximation made simple. *Phys. Rev. Lett.* **1996**, *77*, 3865.
(38) Koelling, D. D.; Harmon, B. N. A technique for relativistic spin-polarised calculations. *J. Phys. C: Solid State Phys.* **1977**, *10*, 3107.
(39) Grimme, S. Semiempirical GGA-type density functional constructed with a long-range dispersion correction. *J. Comput. Chem.* **2006**, *27*, 1787−1799.